Article

Polyoxometalates with Internal Cavities: Redox Activity, Basicity, and Cation Encapsulation in [XPWO] Preyssler Complexes, with X = Na, Ca, Y, La, Ce, and Th

Jorge A. Fernndez, Xavier Lpez, Carles Bo, Coen de Graaf, Evert J. Baerends, and Josep M. Poblet

J. Am. Chem. Soc., **2007**, 129 (40), 12244-12253• DOI: 10.1021/ja0737321 • Publication Date (Web): 14 September 2007

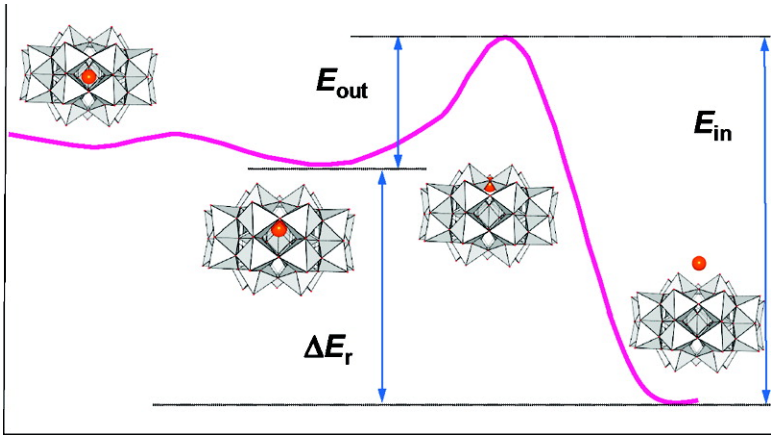

More About This Article

Additional resources and features associated with this article are available within the HTML version:

- Supporting Information
- Links to the 13 articles that cite this article, as of the time of this article download
- Access to high resolution figures
- Links to articles and content related to this article
- Copyright permission to reproduce figures and/or text from this article

View the Full Text HTML

J|A|C|S
ARTICLES
Published on Web 09/14/2007

Polyoxometalates with Internal Cavities: Redox Activity, Basicity, and Cation Encapsulation in $[X^{n+}P_5W_{30}O_{110}]^{(15-n)-}$ Preyssler Complexes, with X = Na^+, Ca^{2+}, Y^{3+}, La^{3+}, Ce^{3+}, and Th^{4+}

Jorge A. Fernández,[†] Xavier López,*[,†] Carles Bo,[†,||] Coen de Graaf,[†,‡] Evert J. Baerends,[§] and Josep M. Poblet*[,†]

Contribution from the Departament de Química Física i Inorgànica, Universitat Rovira i Virgili, Marcel·li Domingo s/n, 43007 Tarragona, Spain, Institució Catalana de Recerca i Estudis Avançats (ICREA), Passeig Lluis Companys 23, 08010 Barcelona, Spain, Divisie Scheikunde, afd. Theoretische Chemie, Vrije Universiteit Amsterdam, De Boelelaan 1083, Amsterdam 1081 HV, The Netherlands, and ICIQ - Institute of Chemical Research of Catalonia, Avda. dels Països Catalans s/n, 43007 Tarragona, Spain

Received May 24, 2007; E-mail: josepmaria.poblet@urv.cat; javier.lopez@urv.cat

Abstract: The Preyssler anion, of general formula $[X^{n+}P_5W_{30}O_{110}]^{(15-n)-}$, is the smallest polyoxometalate (POM) with an internal cavity allowing cation exchange with the solution. The Preyssler anion features a rich chemistry evidenced by its ability to accept electrons at low potentials, to selectively capture various metal cations, and to undergo acid−base reactions. A deep understanding of these topics is herein provided by means of DFT calculations on the title series of compounds. We evaluate the energetics of the release/encapsulation process for several X^{n+} cations and identify the effect of the encapsulated ion on the properties of the Preyssler anion. We revisit the relationship between the internal cation charge and the electrochemical behavior of the POM. A linear dependence between the first one-electron reduction energies and the encapsulated X^{n+} charge is found, with a slope of 48 mV per unit charge. The protonation also shifts the reduction potential to more positive values, but the effect is much larger. In connection to this, the last proton's pK_a = 2 for the Na^+ derivative was estimated to be in reasonable agreement with experiment. The electronic structure of lanthanide derivatives is more complex than conventional POM structures. The reduction energy for the Ce^{IV}-Preyssler + $1e^-$ → Ce^{III}-Preyssler process was computed to be more exothermic than that of very oxidant species such as $S_2Mo_{18}O_{62}^{4-}$.

Introduction

The interest in designing new molecule-based materials that mimic macroscopic devices is growing steadily in the past decades. Properties such as electronic conduction, magnetism, ionic transport, and molecular recognition are key points in the constant search for miniaturization. Within the design and development of nanostructures, the field of polyoxometalates (POMs) is very active.[1−3] Molecules belonging to this family feature unique structural (cavities, channels, networks) and electronic (electron carriers, magnetism) characteristics of technological interest.[4] Two research groups have been especially relevant in the synthesis of medium- and large-sized POMs of increasing structural complexity: Pope's group for isolating a large system composed of 148 tungsten atoms and hundreds of oxygens;[5] and Müller's group, responsible for establishing a new subfamily of ball- and ring-shaped polyoxomolybdates, some of them containing more than 350 Mo atoms.[6] In this line of research, Kortz and collaborators published hybrid organic−inorganic polyanions with ∼1000 atoms featuring hydrophobic cavities of up to 7 Å in diameter.[7] Porous materials

[†] Universitat Rovira i Virgili.
[‡] Institució Catalana de Recerca i Estudis Avançats (ICREA).
[§] Vrije Universiteit Amsterdam.
[||] ICIQ - Institute of Chemical Research of Catalonia.

(1) (a) Alizadeh, M. H.; Razavi, H.; Bamoharram, F.; Hassanzadeh, M. K.; Khoshnavazzi, R.; Zonoz, M. F. *Kinet. Catal*. **2003**, *44*, 524. (b) Harrup, M. K.; Hill, C. L. *Inorg. Chem.* **1994**, *33*, 5448.
(2) (a) Hill, C. L.; Weeks, M. S.; Schinazi, R. F. *J. Med. Chem*. **1990**, *33*, 2767. (b) Rhule, J. T.; Hill, C. L.; Judd, D. A. *Chem. Rev.* **1998**, *98*, 327.
(3) Coronado, E.; Gómez-Garcia, C. J. *Chem. Rev.* **1998**, *98*, 273. Long, D.-L.; Burkholder, E.; Cronin, L. *Chem. Soc. Rev.* **2007**, *36*, 105.
(4) (a) Velessiotis, D.; Glezos, N.; Ioannou-Sougleridis, V. *J. Appl. Phys.* **2005**, *98*, 84503. (b)Wang, Y.; Guo, C.; Chen, Y.; Hu, C.; Yu, W. *J. Colloid Interface Sci.* **2003**, *264*, 176. (c) Oh, S.; Yun, Y.; Kim, D.; Han, S. *Langmuir* **1999**, *15*, 4690. (d) Coronado E.; Mingotaud C. *Adv. Mater. Res*. **1999**, *11*, 869.
(5) (a) Wassermann, K.; Dickman, M. H.; Pope, M. T. *Angew. Chem., Int. Ed.* **1997**, *36*, 1445. (b) Sadakane, M.; Dickman, M. H.; Pope, M. T. *Angew. Chem., Int. Ed.* **2000**, *39*, 2914. (c) Wassermann, K.; Pope, M. T. *Inorg. Chem.* **2001**, *40*, 2763. (d) Sadakane, M.; Ostuni, A.; Pope, M. T. *J. Chem. Soc., Dalton Trans.* **2001**, 63. (e) Kim, K.-C.; Pope, M. T. *J. Chem. Soc., Dalton Trans.* **2001**, 986.
(6) (a) Müller, A.; Kögerler, P.; Kuhlmann, C. *Chem. Commun*. **1999**, 1347. (b) Müller, A.; Shah, S. Q. N.; Bögge, H.; Schmidtmann, M. *Nature* **1999**, *397*, 48. (c) Müller, A.; Serain, C. *Acc. Chem. Res.* **2000**, *33*, 2. (d) Müller, A.; Das, S. K.; Kögerler, P.; Bögge, H.; Schmidtmann, M.; Trautwein, A. X.; Schünemann, V.; Krickemeyer, E.; Preetz, W. *Angew. Chem., Int. Ed.* **2000**, *39*, 3413. (e) Müller, A.; Beckmann, E.; Bögge, H.; Schmidtmann, M.; Dress, A. *Angew. Chem., Int. Ed.* **2002**, *41*, 1162. (f) Müller, A.; Das, S. K.; Talismanova, M. O.; Bögge, H.; Kögerler, P.; Schmidtmann, M.; Talismanov, S. S.; Luban, M.; Krickemeyer, E. *Angew. Chem., Int. Ed.* **2002**, *41*, 579.
(7) Kortz, U.; Hussain, F.; Reicke, M. *Angew. Chem., Int. Ed.* **2005**, *44*, 3773.

10.1021/ja0737321 CCC: $37.00

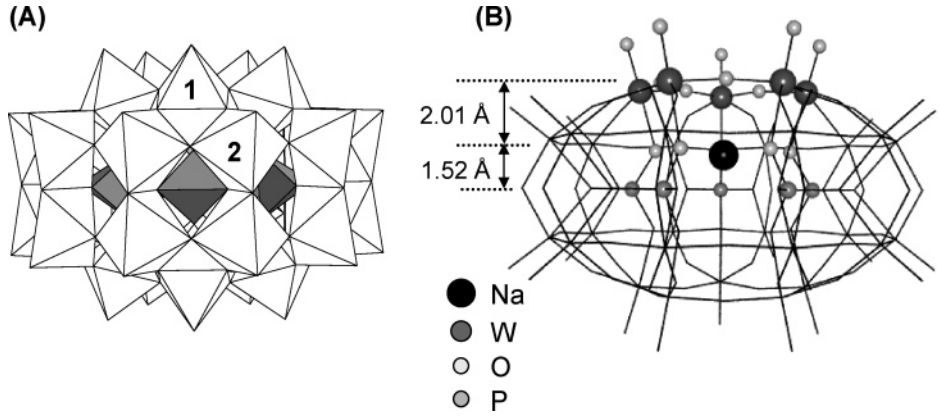

Figure 1. Polyhedral (A) and ball-and-stick (B) views of the Preyssler anion, $[NaP_5W_{30}O_{110}]^{14-}$. The latter shows the internal cavity in which the Na^+ ion is shifted off the center toward a fivefold coordination of oxygen atoms. The values, in Å, give the distances from Na to the planes constituted by five P and five axial W atoms.

based on giant POMs may be used as models for Li^+ transport processes that occur in nature on a cellular level.[8]

Reported for the first time in 1970 by Preyssler[9] and structurally resolved through X-ray diffraction by Pope and co-workers 15 years later,[10] $[NaP_5W_{30}O_{110}]^{14-}$ is a pioneering case of a POM with an internal cavity. The 30 W atoms may be classified as axial and equatorial (labeled 1 and 2 in Figure 1A, respectively). There are 10 axial and 20 equatorial centers distributed in four parallel rings. Its doughnut-shaped structure allows encapsulation of a Na^+ cation (Figure 1B). Later, it was shown that a water molecule is linked to the internal metal ion.[11] This feature is, however, of limited importance for most of Preyssler's properties because the internal water molecule only modifies slightly the orbital energies of the POM framework. The synthesis and structure of $[\{Sn(CH_3)_2\}_4(H_2P_4W_{24}O_{92})_2]^{28-}$ has also been reported.[12] This molecule may be considered a lacunary derivative of the Preyssler anion containing an empty hydrophobic pocket in the center of the cluster.

The central Na^+ cation can be replaced under hydrothermal conditions by other ions of similar size.[13] The anion has proven to be of great help in nuclear waste treatment due to its ability to *selectively* capture lanthanide/actinide cations from neutral aqueous solutions of high salt content.[13d] Cations that have already been incorporated into the internal cavity are trivalent lanthanides such as La^{3+}, Ce^{3+}, Nd^{3+}, Eu^{3+}, etc. and tetravalent actinides, such as U^{4+}.[14] Preyssler anions have also been tested in catalysis.[15] Indeed, many authors put a brilliant future on the Preyssler anion as green catalyst[16] due to its capability to replace the conventional environmentally hazardous and corrosive mineral acids. The analysis of the redox properties of POMs incorporating rare earth atoms is an active research area as well.[17] By means of electrochemical and spectroscopical data, Antonio and co-workers[18] recently illustrated the sequence and energy of the frontier molecular orbitals for $X^{n+}P_5W_{30}O_{110}^{q-}$ Preyssler anions, abbreviated $[XPA]^{q-}$, with X = Na, Ca/Sr, La/Y, and Th. In that work, the authors call for theoretical results on this system to be compared with experimental data.

Over the past decade our group has systematically carried out computational studies on Keggin, Dawson, Lindqvist, and related POM structures.[19] The DFT approach has been shown to be appropriate to reproduce and explain their redox properties, isomer stabilities, and basicities. Other chemical properties such as NMR chemical shifts, IR spectra, magnetism, reactivity, etc. have also been studied theoretically.[20−21] In this paper, we study the structure and electronic properties of the Preyssler anion. The choice of this anion is not arbitrary; its relatively low computational cost (a combination of molecular symmetry and medium size), the presence of an internal cavity, and its redox and catalytic properties make this anion a unique model for the theoretical analysis of some POM properties. In this article we focus our interest on the connection between redox properties and an encapsulated cation, besides other properties as the nucleophilicity of the internal and external surface of the molecule. To the best of our knowledge, this is the first theoretical characterization of the electronic structure of a lanthanide-containing POM. We will show that the charge of the cation determines the energetic cost of uptake and release of ions through a pore in this POM.

(8) (a) Müller, A.; Rehder, D.; Haupt, E. T. K.; Merca, A.; Bögge, H.; Schmidthmann, M.; Heinze-Brückner, G. *Angew. Chem., Int. Ed.* **2004**, *43*, 4466. (b) Haupt, E. T. H.; Wontorra, C.; Rehder, D.; Müller, A. *Chem. Commun.* **2005**, 3912.
(9) Preyssler, C. *Bull. Soc. Chim. Fr.* **1970**, 30.
(10) Alizadeh, M. H.; Harmalker, S. P.; Jeannin, Y.; Martin-Frère, J.; Pope, M. T. *J. Am. Chem. Soc.* **1985**, *107*, 2662.
(11) Kim, K. C.; Pope, M. T.; Gama, G. J.; Dickman, M. H. *J. Am. Chem. Soc.* **1999**, *121*, 11164.
(12) Hussain, F.; Kortz, U.; Keita, B.; Nadjo, L.; Pope, M. T. *Inorg. Chem.* **2006**, *45*, 761.
(13) (a) Antonio, M. R.; Soderholm, L. *Inorg. Chem.* **1994**, *33*, 5988. (b) Lis, S.; Elbanowski, M.; But, S. *Acta Phys. Pol. A* **1996**, *90*, 361. (c) Szyczewski, A.; Lis, S.; Kruczynski, Z.; Pietrzak, J.; But, S.; Elbanowski, M. *Acta Phys. Pol. A* **1996**, *90*, 345. (d) Antonio, M. R.; Williams, C. W.; Soderholm, L. *J. Alloys Compd.* **1998**, *271*, 846.
(14) Dickman, M. H.; Gama, G. J.; Kim, K.-C.; Pope, M. T. *J. Cluster Sci.* **1996**, *7*, 567.
(15) Alizadeh, M. H.; Razavi, H.; Bamoharram, F. F.; Hassanzadeh, M. K.; Khoshnavazi, R.; Zonoz, F. M. *Kinet. Catal.* **2003**, *44*, 524.
(16) (a) Bamoharram, F. F.; Roshani, M.; Alizadeh, M. H.; Razavi, H.; Moghayadi, M. *J. Braz. Chem. Soc.* **2006**, *17*, 505. (b) Bamoharram, F. F.; Heravi, M. M.; Roshani, M.; Tavakoli, N. *J. Mol. Catal. A: Chem.* **2006**, *252*, 219.
(17) (a) Creaser, I. C.; Heckel, M. C.; Neitz, R. J.; Pope, M. T. *Inorg. Chem.* **1993**, *32*, 1573. (b) Antonio, M. R.; Soderholm, L. *J. Alloys Compd.* **1997**, *250*, 541. (c) Liu, S.; Kurth, D. G.; Bredenkötter, B.; Volkmer, D. *J. Am. Chem. Soc.* **2002**, *124*, 12279.
(18) Chiang, M.; Antonio, M. R.; Soderlholm, L. *Dalton Trans.* **2004**, 3562.
(19) (a) Maestre, J. M.; Sarasa, J. P.; Bo, C.; Poblet, J. M. *Inorg. Chem.* **1998**, *37*, 3071. (b) Maestre, J. M.; López, X.; Bo, C.; Casañ-Pastor, N.; Poblet, J. M. *J. Am. Chem. Soc.* **2001**, *123*, 3749. (c) López, X.; Poblet, J. M. *Inorg. Chem.* **2004**, *43*, 6863.
(20) Poblet, J. M.; López, X.; Bo, C. *Chem. Soc. Rev.* **2003**, *32*, 297.
(21) (a) Bagno, A.; Bonchio, M. *Angew. Chem., Int. Ed.* **2005**, *44*, 2023. (b) Quinonero, D.; Wang, Y.; Morokuma. K.; Khavrutskii, L. A.; Botar, B.; Geletii, Y. V.; Hill, C. L.; Musaev, D. G. *J. Phys. Chem. B* **2006**, *110*, 170. (c) Duclusaud, H.; Borshch, S. A. *J. Am. Chem. Soc.* **2001**, *123*, 2825. (d) Bridgeman, A. J. *Chem.—Eur. J.* **2006**, *12*, 2094. (e) Kumar, D.; Derat, E.; Khenkin, A. M.; Neumann, R.; Shaik, S. *J. Am. Chem. Soc.* **2005**, *127*, 17712.

Table 1. Comparison of DFT-Computed and X-ray Distances (in Å) for Some Preyssler $[X^{n+}PA]^{q-}$ POMs under the C_{5v} Symmetry Constrains

	$[NaPA]^{14-}$		$[CaPA]^{13-}$		$[YPA]^{12-}$		$[ThPA]^{11-}$
	expt	DFT	expt	DFT	expt	DFT	DFT
W−O_t	1.71	1.78	1.72	1.78	1.71	1.75	1.76
W−O_b	1.80−2.08	1.91−1.99	1.83−1.96	1.93−1.98	1.86−1.97	1.91−1.95	1.89−2.00
W−O_p	2.25	2.25	2.26	2.32	2.26	2.42	2.33
X−O_p	2.64	2.74	2.70	2.61	2.60	2.47	2.64
d(X−plane)[a]	-	0.923	-	1.172	-	1.541	1.945
d(X−plane)[a,b]	1.55	1.53	1.49	1.49	1.44	1.44	1.67

[a] Distances between the internal cation X and the equatorial plane. [b] Calculations with the C_s model containing a water molecule coordinated to the internal cation.

Computational Details

DFT calculations presented here were performed with the ADF2004.01 package.[22] We applied the local density approximation featuring the Xα model with Becke's functional[23] for exchange and the VWN parametrization[24] with Perdew's correction[25] for correlation. Geometry optimizations were carried out in the gas phase using a Slater TZP-quality basis set to describe the valence electrons of high-symmetry compounds (D_{5h} and C_{5v}) and a DZ-type one for low-symmetry systems (C_s or C_1). Thereafter, we carried out single-point COSMO[26] calculations to account for the solvent effects (water, $\epsilon = 78.4$) with a TZP-quality basis set for all the gas-phase converged geometries. To define the cavity surrounding the anions, we applied the solvent-excluding method with a fine tesserae.[27] The ionic radii for the POM atoms, which actually define the cavity in the COSMO, are 1.26, 1.52, 1.00, and 1.14 Å for W^{6+}, O^{2-}, P^{5+}, and Na^{+}, respectively. The core electrons (O, 1s; P, Na, 1s-2s; V, 1s-2p; W, 1s-4d; Y, 1s-3d; La, 1s-4d; Ce, 1s-4d; Th, 1s-5d) were kept frozen and described by single Slater functions. We applied scalar relativistic corrections to them, the zeroth-order regular approximation (ZORA), via the core potentials generated with the DIRAC program.[22] Monoreduced species were computed at the geometry optimized for the oxidized partner using the unrestricted formalism.

Results and Discussion

1. Location and Exchange of the Central Cation. High level quantum-mechanical calculations of large molecules are, in general, very computationally demanding. However, most codes are adapted to take advantage of molecular symmetry, decreasing the computational requirements. The Preyssler framework $[NaP_5W_{30}O_{110}]^{14-}$ has a nearly D_{5h} symmetry (see Figure 1) when Na is at the geometrical center of the structure. However, X-ray and EXAFS studies show that Na does not lie at the center but is actually displaced along the vertical [circ]-C_5 axis.[10−11,28] Hence we consider three different models for computation: (1) the highly symmetrical D_{5h} cluster, with the internal cation in the geometrical center of the cavity, (2) the C_{5v} symmetry compound, with the internal cation shifted off from the center, and (3) a low symmetry C_s cluster, with an encapsulated water molecule that just leaves a vertical plane of symmetry. In the D_{5h} model system, the internal Na^+ cation and five P atoms surrounding it are contained in the equatorial σ_h symmetry plane, which avoids reproducing the experimental position of the Na cation, although the computed geometry of the external cage is correct. Releasing the σ_h symmetry restrictions improves the structural parameters related to the position of Na^+ (see Figure 1B). Nevertheless, the distance found between the cation and the equatorial plane does not yet completely agree with the X-ray data. Only the inclusion of the explicit water molecule inside the cluster, bound to the internal cation, generating a C_s symmetry compound $[|XH_2O|PA]^{q-}$, leads to the correct position of the encapsulated cation. Table 1 summarizes the main interatomic distances in the C_{5v} cluster, where O_t is the terminal oxygen, O_b is the bridging oxygen, O_p is the oxygen linked to a phosphorus atom, and X is the internal cation. The water unit pushes the internal cation further off the center of the cavity to the correct position. However, the price to pay is a dramatic increase in the computational effort. Therefore, some of the properties in this work have been studied using the C_{5v} symmetry point group with the internal cation, X^{n+}, shifted off the center, but without the water unit. It is shown below in this paper that this approximation does not affect the validity of the data.

There is evidence that Preyssler anions encapsulate cations selectively, even though these are interchangeable in solution only if certain conditions of temperature are reached. To further rationalize this point, we address the energies involved in the process of cation release. As such, we may identify the $\hat{C}_5$ axis as a plausible migration path for the title X^{n+} cations. The study was carried out as a *dynamic scan*. It consisted in a set of geometries in which X^{n+} was fixed on the $\hat{C}_5$ axis at steps of 0.5 Å. Each geometry was re-optimized under the C_{5v} symmetry constrains keeping the position of X^{n+} frozen.[29] In the first point of the scan, X^{n+} was in the equatorial plane. The last point was computed as two independent systems: free POM and X^{n+} solvated units.

Figure 2 shows the energy profiles obtained for the set of X^{n+} cations, in which we identify different regions along the release path. First is the structure with D_{5h} symmetry in which the path presents a local maximum; when the cation starts to move along the axis, the total energy slightly decreases to ca. −20 kcal mol^{-1} for Th^{4+} and Y^{3+}, leading to an energy

(22) (a) ADF 2004.01. Department of Theoretical Chemistry. Vrije Universiteit. Amsterdam. Baerends, E. J.; Ellis, D. E.; Ros, P. *Chem. Phys.* **1973**, *2*, 41. (b) Versluis, L.; Ziegler, T. *J. Chem. Phys.* **1988**, *88*, 322. (c) Te Velde, G.; Baerends, E. J. *J. Comput. Phys.* **1992**, *99*, 84. (d) Fonseca Guerra, C.; Snijders, J. G.; Te Velde, G.; Baerends, E. J. *Theor. Chem. Acc.* **1998**, *99*, 391.
(23) (a) Becke, A. D. *J. Chem. Phys.* **1986**, *84*, 4524. (b) Becke, A. D. *Phys. Rev.* **1988**, *A38*, 3098.
(24) Vosko, S. H.; Wilk, L.; Nusair, M. *Can. J. Phys.* **1980**, *58*, 1200.
(25) (a) Perdew, J. P. *Phys. Rev.* **1986**, *B33*, 8822. (b) Perdew, J. P. *Phys. Rev.* **1986**, *B34*, 7406.
(26) (a) Klamt, A.; Schüürmann, G. *J. Chem. Soc., Perkin Trans.* 2 **1993**, 799. (b) Andzelm, J.; Kölmel, C.; Klamt, A. *J. Chem. Phys.* **1995**, *103*, 9312. (c) Klamt, A. *J. Chem. Phys.* **1995**, *99*, 2224. Method implemented in the ADF package by (d) Pye, C. C.; Ziegler, T. *Theor. Chem. Acc.* **1999**, *101*, 396.
(27) Pascual-Ahuir, J. L.; Silla, E.; Tuñón, I. *J. Comput. Chem.*, **1994**, *15*, 1127.
(28) Chiang, M.-H.; Antonio, M. R.; Williams, C. W.; Soderholm, L. *Dalton Trans.* **2004**, 801.

(29) The energy at each point corresponds to a single-point TZP/COSMO calculation performed with the gas-phase optimized geometry using a DZP basis set.

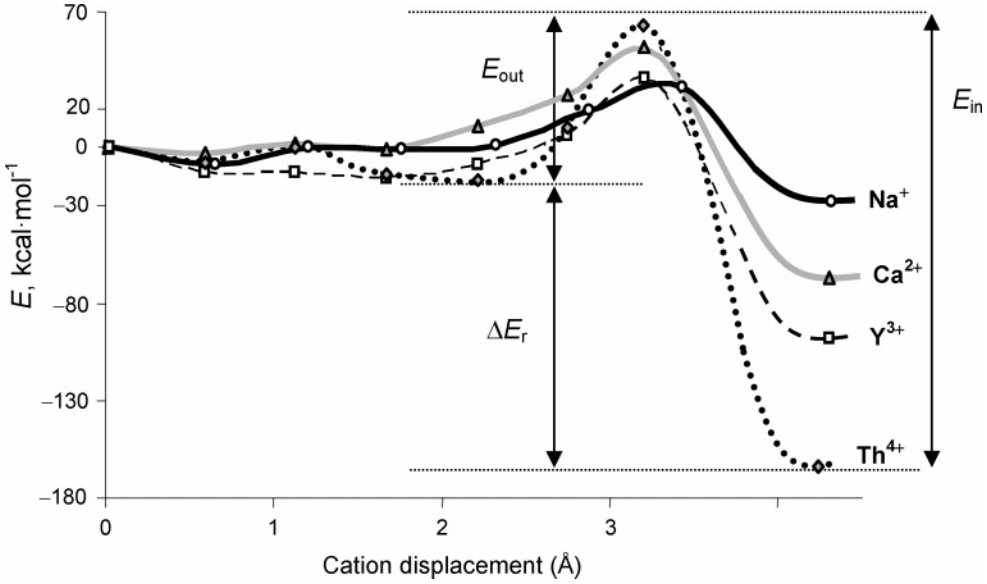

Figure 2. Energy profiles for the release of Na^+, Ca^{2+}, Y^{3+}, and Th^{4+} in $X^{n+}P_5W_{30}O_{110}^{(15-n)-}$ obtained from *dynamic scans*. The horizontal axis represents the distance of X^{n+} to the equatorial plane of the cluster, and the vertical axis, the energy relative to the starting point. The rightmost points have been computed considering two independent units, so the horizontal scale is only approximate after 3.5 Å (see text for details).

Table 2. Computed Energies Involved in Cation Exchange (in kcal/mol),[a] Experimental Hydration Energies, and Temperatures of Synthesis for Each X

	computed			experimental[b]	
X	ΔE_r	E_{in}	E_{out}	ΔG_{hyd}	T (°C)
Na^+	18.6	58.0	39.4	−87	120
Ca^{2+}	61.5	112.1	50.6	−360	140
Y^{3+}	81.1	128.2	47.1	−825	160
Th^{4+}	145.0	215.2	69.2	−1391	238[c]

[a] ΔE_r, reaction energies; E_{in}, encapsulation energy barriers; E_{out}, release energy barriers. [b] Data from ref 14. [c] Data from ref 18.

minimum at cation displacements of approximately 1.5 and 1.9 Å for the trivalent and tetravalent cations, respectively (see Table 1). These points correspond to a stabilizing interaction with the five O_p oxygens. For Na^+, the stabilization is 8 kcal mol^{-1}, and Ca^{2+} features only a slight energy decrease at ca. 0.5 Å. Then, the motion of the internal cation along the vertical axis entails a remarkable destabilization of the system for all X^{n+}, reaching a maximum in the region at ca. 3.5 Å from the starting point. At this point, X^{n+} lies on the plane of the axial W_5 ring. The diameter of this ring is 5.6 Å and defines a sort of window of the cavity, containing five bridging oxygens pointing toward the cation. For Ca^{2+}, the energy barrier (E_{out}) is 50.6 kcal mol^{-1}, comparable to the energy computed for Y^{3+} and 11.2 kcal mol^{-1} higher than that for Na^+. For the tetravalent Th^{4+} $E_{out} = 69.2$ kcal mol^{-1} (see Table 2 and Figure 2). These large energies are caused by the loss of the stabilizing interaction between the cation and the POM, which is mainly electrostatic (see Figure S3). When the cation approaches the window there is some deformation of the W_5O_5 ring: the oxygen atoms move toward the cation and the highly charged W^{6+} ions move away. At the top of the barrier some computed distances are as follows: $d(Na^+-O_b) = 2.357$ Å and $d(Th^{4+}-O_b) = 2.295$ Å, whereas $d(Na^+-W)$ and $d(Th^{4+}-W)$ are 3.295 and 3.441 Å, respectively (Chart 1).

In Figure 2, distances larger than ∼3.5 Å actually represent the situation where X^{n+} has left the $P_5W_{30}O_{110}$ fragment, and both become independent units. Notice that the ensemble

Chart 1

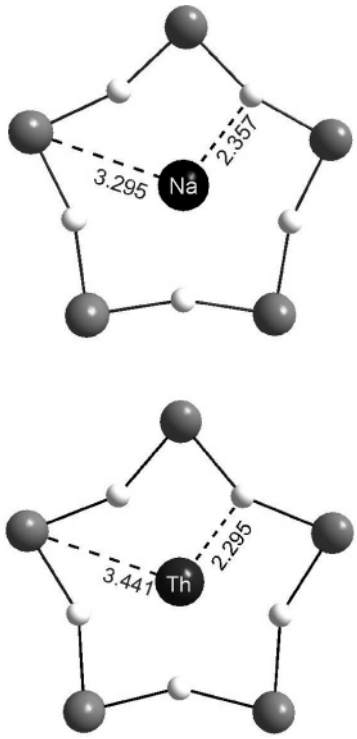

stabilizes dramatically in that region and that such stabilization is more important for higher cation charges. Our calculations associate this increasing stabilization mainly to the solvation of X^{n+}. Computing the energies at the last point is not straightforward since calculating accurate values of solvated small cations is a difficult task. To tackle this important point we used experimental solvation energies for the free cations discussed here.[30] Hence, the energy at the last point in our dynamic scan has been obtained as the sum of the theoretically calculated cation-free Preyssler framework plus the energy of

(30) Marcus, Y. *J. Chem. Soc., Faraday Trans.* **1991**, *87*, 2998.

the free solvated cation. The latter was computed as the sum of the quantum mechanical energy of the cation in gas phase and its experimental hydration energy.[30] This scheme allows us to estimate the reaction energy ΔE_r for the full way out of a cation from the interior of a Preyssler anion. E_{in} is herein defined as the energy barrier to encapsulate a solvated cation. The internal water molecule has not been considered in this part of the study assuming that the cation release most probably involves the breaking of the cation$-H_2O$ bond and then the cation alone leaves the POM.

These energy paths also provide information about the energies involved in the cation substitution. It is known that XPA compounds are obtained from heating a $NaPA^{14-}$ solution in the presence of other X^{n+}.[14] From our results, Na^+ needs about 40 kcal mol^{-1} to be released, which explains the high temperature (120 °C) required for a considerable cation exchange. The Na-free POM may then uptake a free cation. Encapsulations of Ca^{2+}, Y^{3+}, and Th^{4+} are very endothermic processes of 61, 81, and 145 kcal mol^{-1}, respectively. The energy barriers of encapsulation for the different cations, E_{in}, provide an estimate to the tendency of the Preyssler anion to capture them since they correlate with the temperatures of synthesis. The $CaPA^{13-}$ is formed at 140 °C in 90% yield, and the synthesis of YPA^{12-} requires even 20 °C more, in agreement with $E_{in} = 112.1$ and 128.2 kcal mol^{-1} calculated for Ca^{2+} and Y^{3+}, respectively. The high encapsulation barrier for $ThPA^{11-}$ (215 kcal mol^{-1}) is in line with the reported conditions of synthesis; 238 °C/96 h.[18] The dehydration energy, which strongly increases with the cation charge, seems to play an important role in the selective encapsulation of cations exhibited by the Preyssler framework.

The monosubstituted $NaP_5VW_{29}O_{110}^{15-}$ cluster, reported by Pope and co-workers,[10] has two structural isomers. The replacement of an axial W gives rise to form **A**, which is slightly more stable than form **B** (equatorial substitution, labels 1 and 2 in Figure 1A). Our calculations favor isomer **A** by 11 kcal mol^{-1}, in agreement with experience. E_{out} for Na^+ in isomer **A** has been computed as exposed above leading to a value 3 kcal mol^{-1} lower than the barrier of P_5W_{30}. This suggests that the incorporation of lower valent cations in axial positions may modestly favor ion exchange.

2. Effect of the Encapsulated Cation on the Electronic Structure of the POM. The electronic structure of $[XPA]^{q-}$ anions is equivalent for any X. The nature of the molecular orbitals is in general delocalized, indicating that most positions are chemically equivalent. In general, the highest occupied molecular orbitals are oxygen p-like (oxo *band*), and the set of lowest unoccupied orbitals are metal d-like (metal *band*). It should be noted that the term *band* is not strictly correct because the molecular orbitals are separated by discrete energies in these medium-sized clusters. The structure of the Preyssler anion features two discernible metal sites: 10 axial (labeled 1 in Figure 1) and 20 equatorial (labeled 2). This has implications in the ordering of molecular orbitals. The lowest unoccupied molecular orbital (LUMO) is mainly delocalized over the axial metals, whereas the subsequent molecular orbitals belong to the equatorial metals (see Supporting Information), indicating that the first electron reduction occurs in the axial region. In the $P_2W_{18}O_{62}^{6-}$ Dawson cluster, the first reduction occurs in the equatorial region, and it could be argued that the two results contradict each other. This is, however, not the case. The LUMO of tungsten-based POMs is normally delocalized over those metal centers that are connected to each other by large W$-$O$-$W angles.[31] The largest W$-$O$-$W angles (150° to 165°) are found in different regions for Preyssler clusters (doughnut-shaped) and Wells$-$Dawson clusters (cylinder-shaped).

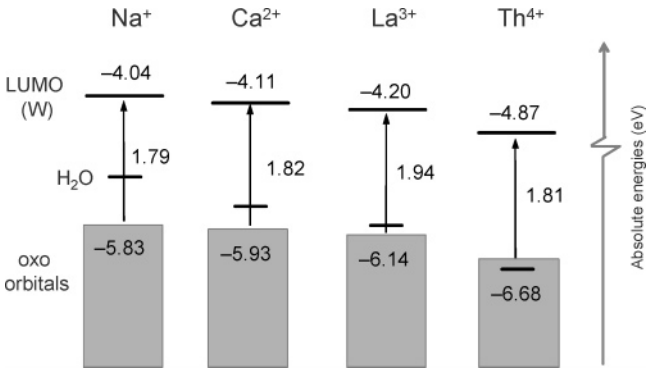

Figure 3. Effect of the internal cation on the frontier orbital energies for $[|XH_2O|\subset PA]^{n-}$ (C_s).

The oxidizing power of a series of Preyssler-type anions can be rationalized by the analysis of their LUMO energies, analogously to other POMs.[35] We can see in Figure 3 that higher cation charges make the LUMO more stable and, consequently, the compound more stable. The orbital energies shown correspond to C_s structures with the water molecule linked to the internal cation. The encapsulated water entails the insertion of the oxygen lone pair between the oxo and the metal bands. This lone pair is also stabilized by the positive charge of the cation. Hence, this orbital appears 0.79 eV above the oxo band for Na^+, 0.17 eV for Ca^{2+}, and below the oxo band for the most charged cation Th^{4+}. The energy gap between the oxo and metal bands agrees with the results found for the lowest charge-transfer excitation, which increases with the charge of the cation.[4]

3. Simulating Reduction Peaks of a Cyclic Voltammogram. Several works throughout the years have evidenced the dependence of the voltammetric data on the charge of ions in solution. Concerning POMs, Pope illustrated the linear dependence of the reduction potentials vs the anion charge for a set of Keggin anions.[32a] The reduction potentials may be estimated theoretically by calculating the fully oxidized molecule and its one-electron reduction partner.

Pope and co-workers observed that the first reduction, $NaPA^{14-} + e^- \rightarrow NaPA^{15-}$, appears at 0.019 V (pH = 1) and -0.173 V (pH > 2.5) vs NHE.[17] The observed gap of 192 mV comes from the different protonation degree in either case. Protonation implies a larger oxidizing power due to a smaller negative charge, explaining the more positive potential at low pH. More recently, Antonio and co-workers have analyzed in detail the dependence of the electrochemical response in XPA clusters on the central ion. The authors observed that the variation of the redox potential per charge unit is 41 mV.[18] In this section, we will show how to reproduce the electrochemical

(31) López, X.; Bo, C.; Poblet, J. M. *J. Am. Chem. Soc.* **2002**, *124*, 12574.
(32) (a) Pope, M. T.; Varga, G. M. *Inorg. Chem.* **1966**, *5*, 1249. (b) Altenau, J. J.; Pope, M. T.; Prados, R. A.; So, H. *Inorg. Chem.* **1975**, *14*, 417.
(33) Lewis, A.; Bumpus, J.; Truhlar, D.; Cramer, J. *J. Chem. Educ.* **2004**, *81*, 596.
(34) Alternau, J. J.; Pope, M. T.; Prados, R. A.; So, H. *Inorg. Chem.* **1975**, *14*, 417.
(35) López, X.; Fernández, J. A.; Poblet, J. M. *Dalton Trans.* **2006**, 1162.

Table 3. Experimental ($E_{1/2}$) and Theoretical (E_c) Absolute Values for the First Cathodic Peaks (in V) for the XPA^{q-} Preyssler-Type Clusters, with X = Na, Ca, La, Th (RE Stands for Reduction Energy)

	$E_{1/2}$ vs (NHE)	*RE* (eV)	E_c vs (NHE)[c]	$\Delta(E_{1/2} - E_c)$[d]
$[NaPA]^{14-}$	0.019[a]	−3.929	−0.430	0.449
$[CaPA]^{13-}$	0.053[a]	−3.963	−0.396	0.449
$[LaPA]^{12-}$	0.096[a]	−4.007	−0.352	0.448
$[ThPA]^{11-}$	0.145[a]	−4.063	−0.296	0.441
$[HNaPA]^{13-}$	−0.053 (pH = 1.5)[b]	−4.043	−0.317	0.264
$[NaPA]^{14-}$	−0.173 (pH = 2.5)[a,b]	−3.929	−0.431	0.258

[a] Data from ref 18. [b] Data from ref 10. [c] Predicted absolute potential vs NHE using Cramer *absolute zero potential*. [d] Difference between the computed and experimental potentials

behavior of a polyoxometalate and that the dependence of the redox potential on the charge is different for *protonation* than for *ion encapsulation*. The theoretical estimation of the redox potential of a given POM requires the determination of the free energy associated with the process.

$$POM_{ox}(aq) + 1e^- \xrightarrow[\Delta G]{} POM_{red}(aq) \qquad (1)$$

Given that the reduction process of a POM involves the addition of one electron to an almost nonbonding orbital, the entropic and vibrational contributions to ΔG in eq 1 can be replaced by its electronic contribution in solution, the reduction energy (RE). As in electrochemical data in which the normal hydrogen electrode (NHE) is taken as the zero on the relative scale, the theoretical values need to be referred to an *absolute theoretical zero*. Cramer et al. have recently[33] recalculated this *absolute zero* to be 4.36 eV for the free energy change in the NHE reaction: $^1/_2\ H_2 \rightarrow H^+ + e^-$.

We analyzed the effect of the encapsulated cation on the redox potential. Table 3 summarizes the first one-electron reduction energies for $[XPA]^{q-}$ (with X = Na^+, Ca^{2+}, La^{3+}, and Th^{4+}) and their relationship with the experimental first reduction peaks. Half-wave potentials vs NHE and theoretical estimates of the reduction energy are shown in the first and second columns, respectively. We observe that reduction energies are more negative (more favorable) for lower anion charges. With the equation $E° = -\Delta G°/nF$ and the Cramer value 4.36 eV, we determined the cathodic peaks (E_c) for Preyssler clusters. Large discrepancies with experimental data were found, although the differences between half-wave potentials and computed values are fairly constant, ∼0.44 eV. Figure 4 contains a plot for the calculated reduction energies for the series $[XPA]^{q-}$ with X = Na^+, Ca^{2+}, La^{3+}, Th^{4+}, and none. The slope of the linear function is 48.3 meV per unit charge, in excellent agreement with the 41.2 mV observed experimentally. Notice that 1 mV corresponds to 0.02 kcal mol^{-1} only, and hence the difference between the theoretical and the experimental slopes is almost negligible, 0.16 kcal mol^{-1}. This linear dependence shows that substitution of the internal cation has purely electrostatic effects on the cluster—a mere shift of the absolute orbital energies—and the geometry and electronic structure remain practically unchanged.

A previous electrochemical study performed for a set of isostructural Keggin ($XW_{12}O_{40}^{n-}$) anions showed a slope of 160 mV per unit charge.[34] These data confirm two fundamental facts: (i) the first reduction step becomes more difficult as the overall anion charge increases, and (ii) the slope depends on the electron density of each POM anion.[35] Changes induced by the addition of one electron to the Preyssler structure are small compared with those induced in smaller polyoxoanions.

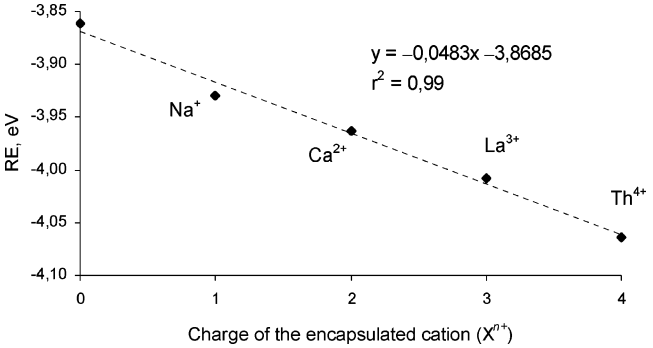

Figure 4. Linear dependence between the charge of the encapsulated X^{n+} cation and the calculated reduction energy (RE) for $[X^{n+}P_5W_{30}O_{110}]^{(15-n)-}$.

As stated before, the degree of protonation of the cluster is an important factor to be considered in the comparison of theoretical and experimental values. There is experimental evidence that the Preyssler anion at pH = 0 is, at least, doubly protonated in the external framework and monoprotonated in the internal cavity. Pope stressed the dependence of reduction waves with the acidity of the solution; at pH = 2.5, the first one-electron reduction peak appears at −0.173 V. At pH = 1.5, the same wave shifted to −0.053 V (see Table 3). Apparently, the Preyssler anion gets protonated between pH 2.5 and 1.5 since a more positive reduction potential must come from a decrease of the total anion charge, that is, from protonation. We have compared the theoretical redox potentials for the protonated and deprotonated compounds with the voltammetric values obtained at different pH's. The computed reduction energy of $[HNaPA]^{13-}$ (protonated in the cavity, see section 4) is −4.04 eV, which is more negative than that of $[NaPA]^{14-}$, in agreement with Pope's measurements. Assuming that the potential shift caused by each proton is 0.12 V, the threefold protonated Preyssler cluster would exhibit a theoretical value of $-4.36 + 3.929 + (3 \times 0.12)$ $V = -0.07$ V vs NHE, very close to the measured 0.019 V (see Table 3). Notice that both protonation and cation encapsulation shift the potential toward more positive values, but this effect is about three times larger in the case of protonation, probably due to the more pronounced geometry changes in the latter case.

4. Nucleophilicity of the Oxygen Sites. The Preyssler anion possesses some exceptional characteristics to act as catalyst, such as the reversible redox chemistry at low potentials, the high hydrolytic stability, or the fast reoxidation by O_2 in both aqueous and nonaqueous media.[36] The first step in many of these catalytic processes involves attachment or release of protons. Therefore, the catalytic activity of POMs is usually connected to their acid strength. Different methods can be used to describe the basicity of molecules. A cheap, qualitative, visual method to capture the local polarity of a molecule consists in plotting the electrostatic potential (EP) over an electron density isosurface to get a molecular electrostatic potential (MEP) representation. The values taken by the EP at each point are coded by colors: red-yellow for nucleophilic regions and green-blue for electrophilic regions. Thus, protons are stabilized by an attractive

(36) Harrup, M. K.; Hill, C. L. *Inorg. Chem.* **1994**, *33*, 5448.

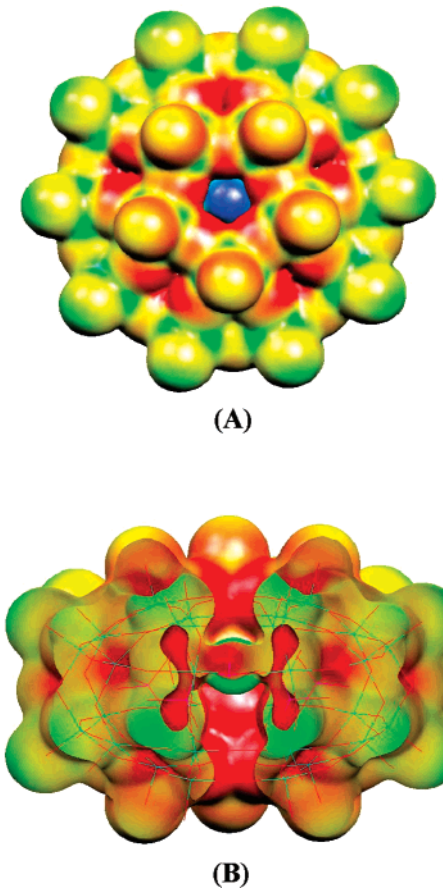

Figure 5. Top (A) and side (B, one-half of the molecule) views of the MEP distribution for $[NaP_5W_{30}O_{110}]^{14-}$. The cavity is the most nucleophilic part (B, red region), where the cation is fully stabilized (Na^+ in this case, easily identified in A by its blue color).

interaction with negative EP (nucleophilic) regions. Figure 5 shows two views of the MEP distribution for $[NaPA]^{14-}$.

In POMs, there are two main structural types of oxygen sites, bridging OM_2 and terminal OM sites, which are susceptible to protonation. However, the less common molecular Preyssler structure featuring a cavity has yet another type of oxygen site accessible for protonation, namely, the oxygen bound to the P atom, O_p.[37] The MEP analysis predicts that the O_p oxygen should be the most basic in the whole cluster (red area in Figure 5B) and that W−O−W oxygens in the axial region are more nucleophilic than the equatorial W−O−W ones. Terminal oxygens OW are the least basic as usual in POMs.[31,38] The internal cation, in this case Na^+, is identified in blue at the center of the cavity (Figure 5A).

To study the nucleophilicity of the oxygen sites in a quantitative way we perform calculations on the protonated molecule. The protonation energy, PE, is computed as the energy difference between products ($HNaPA + H_2O$) and reactants ($NaPA + H_3O^+$) involved in the acid−base reaction. The computed PEs, summarized in Figure 6, confirm the predictions based on the MEP analysis, that is, the most stable HNaPA species features a protonated O_p site, the internal oxygen linked to a phosphorus atom. It is followed by protonation of the

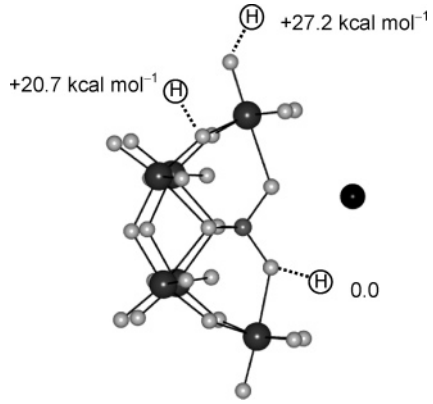

Figure 6. Ball-and-stick representation of three possible protonation sites in the Preyssler anion. Only one of the five equivalent W_6 moieties is shown for clarity. Color code: light gray - oxygen; dark gray - W; gray - P; black - Na. The hydrogen atom is labeled H.

bridging W−O−W oxygen, +20.7 kcal mol^{-1} higher in energy, and, finally, protonation of the terminal O=W oxygen, with +27.2 kcal mol^{-1}.

It is interesting to derive absolute proton affinities theoretically and link them with experimental pK_a values. This requires the determination of the free energy associated with the acid−base reaction shown in eq 2. The pK_a is related to the free energy through the equation $\Delta G_{(aq)} = -2.303RT \log K_a$. As mentioned above, the calculation of the vibrational frequencies is still prohibitive for molecules of such size. Therefore, again we must assume that in the POM species[32] the changes in the entropic and enthalpic terms are small in eq 2.

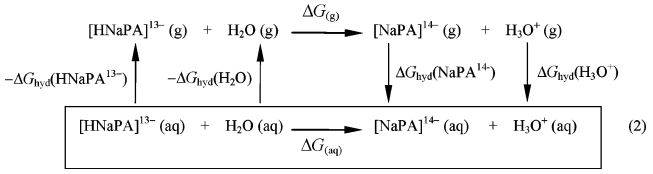

ΔG(aq) can be decomposed into the free energy change in the gas phase, ΔG_g, and $\Delta(\Delta G_{hyd})$, which represents the following change in free energy:

$$\Delta(\Delta G_{hyd}) = \Delta G_{hyd}(NaPA^{14-}) - \Delta G_{hyd}(HNaPA^{13-}) + \Delta G_{hyd}(H_3O^+) - \Delta G_{hyd}(H_2O) \quad (3)$$

In summary, to determine $\Delta G_{(aq)}$ we have to compute the free energies of the polyoxo species as well as H_2O and H_3O^+. The experimental determination of the energies of charged aqua species is rather inaccurate.[39] Experimental estimates of ΔG_{hyd}-(H_3O^+) have been reported in a range between −104.0 and −110.2 kcal mol^{-1} and corresponding to an uncertainty of four pK_a units. Trying to tackle this important shortcoming, many groups have computed the energies of $H_{2n}O_n$ and $H_{2n+1}O_n^+$ cluster models.[40] A recent study, performed at the G2/MP2 and IEF/PCM level,[41] gives an accurate estimate of $\Delta G_{hyd}(H_3O^+)$ = −107.0 kcal mol^{-1}, clearly within the range of experimental values.[39] Applying this value in combination with $\Delta G_{hyd}(H_2O)$

(37) Kim, K.-C.; Pope, M. T.; Gama, G. J.; Dickman, M. *J. Am. Chem. Soc.* **1999**, *121*, 11164.
(38) Kempf, J. Y.; Rohmer, M.-M.; Poblet, J. M.; Bo, C.; Bénard, M. *J. Am. Chem. Soc.* **1992**, *114*, 1136.
(39) (a) Pearson, R. G. *J. Am. Chem. Soc.* **1986**, *108*, 6109. (b) Marcus, Y. *Ion Solvation*; Wiley: New York, 1985. (c) Rashin, A. A.; Honig, B. *J. Phys. Chem.* **1985**, *89*, 5588.
(40) Tawa, G. J.; Topol, I. A.; Burt, S. K.; Caldwell, R. A.; Rashin, A. A. *J. Chem. Phys.* **1998**, *109*, 4852 and ref 13 therein.
(41) Jitariu, L. C.; Masters, A. J.; Hillier, I. H. *J. Chem. Phys.* **2004**, *121*, 7795.

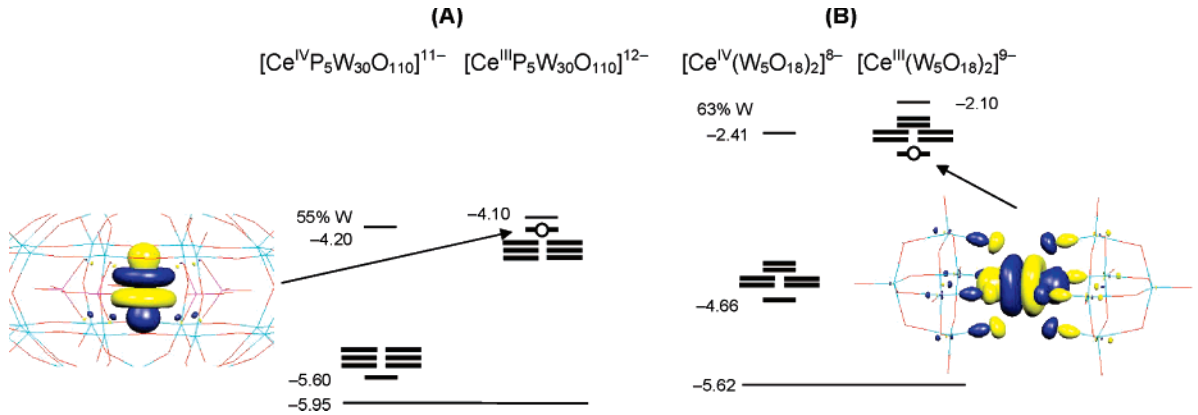

Figure 7. Comparison of two POM complexes containing Ce. (A) $[Ce^{IV,III}P_5W_{30}O_{110}]^{11/12-}$ and (B) $[Ce^{IV,III}(W_5O_{18})_2]^{8/9-}$. Thin and thick lines are molecular orbitals with major W or Ce character, respectively. The long lines at the bottom represent the highest occupied oxo orbital. Empty circles are electrons. Relevant absolute orbital energies are shown in eV. The colored molecular orbitals are those accepting the electron in either case. In (A, where only the internal Ce-PA cavity is shown for clarity) it is 97% Ce-f and 3% O-p, whereas in (B) it has 90% Ce-f character and 10% O-p character. See text for further details.

$= -6.3$ kcal mol^{-1} [42] leads to $\Delta G_{(aq)} = \Delta G_{(g)} + \Delta(\Delta G_{hyd}) = -2.67$ kcal mol^{-1} and

$$pK_a = -\log K_a = \Delta G_{(aq)}/(2.303RT) = 1.96$$

for $HNaPA^{14-}$ at room temperature. This pK_a corresponds to the release of a proton from the internal O_p site and explains the different electrochemical responses at pH = 1.5 and 2.5 described above. In conclusion, computed protonation free energies and reduction properties fully confirm that there is a protonation of $NaPA^{14-}$ at pH values below 2.0.

5. Lanthanide−POM Complexes. The first reports on Ln−POM structures date from the early past century with the study of the 12-molybdocerate(IV) by Barbieri,[43] also studied by Baker and others.[44] Those reports are mainly structural, stressing the superacid character of the free acid and its possible associated interest. Peacock and co-workers started the synthesis of $[Ce^{IV/III}(W_5O_{18})_2]^{8/9-}$ structures.[45] Dawson clusters containing rare earth atoms have been also extensively studied, notably by Francesconi and co-workers.[46] Other authors have also extensively studied $[Ln^{x+}P_5W_{30}O_{110}]^{n-}$ using spectroscopic and voltammetric data,[13a,47] but at present, there is neither computational information about the sequence of the molecular orbitals nor the electron distribution at the Ln center, even if some important questions remain unsolved. These are, among others, the electrochemical response of Ce−POM complexes and the oxidation states they feature in different structures. The incorporation of cationic cerium into a Preyssler cavity was reported by Pope,[17a] proposing that the oxidation state of Ce is IV. Later, Antonio et al. demonstrated from EXAFS measurements that in fact the oxidation state of the cerium ion inside the P_5W_{30} cluster is III.[13d] Evans has shown in a recent didactic paper that the misunderstandings in the f element chemistry have not been infrequent in the past century.[48] We herein try to give a theoretical viewpoint to this question.

Quantum mechanical calculations have shown to be helpful in the analysis of most complex structures, but the theoretical study of Ln−POM clusters is rather problematic because the maximum in the radial distribution of the f shell is close to the nuclei. That is why it is often considered a core shell, although its energy corresponds to the region of the frontier molecular orbitals. The first question we try to unravel is why some POM clusters incorporate either Ce^{III} *or* Ce^{IV} and other POMs both. Our interest is focused on $[Ce^{IV,III}P_5W_{30}O_{110}]^{11/12-}$ (Ce-Preyssler), notably what is the preferred oxidation state for Ce and why. For this purpose, we computed both $Ce^{III,IV}$ molecules incorporating the solvent effects. The results are schematically presented in Figure 7A. In the fully optimized structure computed under the constraints of the C_{5v} symmetry the internal cerium cation is displaced 0.553 Å off the equatorial plane. The LUMO of the oxidized Ce-Preyssler complex is a pure Ce-4f(z^3) orbital with an energy of −5.60 eV, only 0.35 eV above the oxo band, which we interpret as evidence of instability of the oxidized form. Our DFT calculations indicate that the metal-oxide framework (and notably the internal cavity) is not able to coordinate the Ce covalently, leading to long Ce−O distances of ca. 2.72 Å. Besides that, only five oxygens are directly linked to the Ce atom, which is a relatively poor coordination. Both the pure character of the Ce orbitals (97% 4f) and the relatively long Ce−O distances encountered are typical of a mere electrostatic interaction between Ce and O.

(42) Ben-Naim, A.; Marcus, Y. J. *Chem. Phys.* **1984**, *81*, 2016.
(43) Barbieri, G. A. *Atti. Accad. Lincei* **1914**, *5*, 805.
(44) (a) Baker, L. C. W.; Gallagher, G. A.; McCutcheon, T. P. *J. Am. Chem. Soc.* **1953**, *75*, 2493. (b) Dexter, D. D.; Silverton, J. V. *J. Am. Chem. Soc.* **1968**, *90*, 3589. (c) Tat'ganina, I. V.; Chernaga, F. S.; Torchenkova, E. A.; Simonox, V. I.; Spitsyn, V. I. *Dokl. Chem.* **1979**, *247*, 387. (d) Inoue, M.; Yamase, Y. *Bull. Chem. Soc. Jpn.* **1995**, *68*, 3055.
(45) (a) Peacock, R. D.; Weakley, T. J. R. *J. Chem. Soc. A* **1971**, *11*, 1836. (b) Peacock, R. D. *J. Chem. Soc. A* **1971**, *12*, 2028. (c) Peacock, R. D.; Weakley, T. J. R. *J. Chem. Soc. A* **1971**, *12*, 1937.
(46) (a) Bartis, J.; Dankova, M.; Lessmann, J. J.; Luo, Q.-H.; Horrocks, W. DeW., Jr.; Francesconi, L. C. *Inorg. Chem.* **1999**, *38*, 1042. (b) Luo, Q.-H.; Howell, R. C.; Dankova, M.; Bartis, J.; Williams, C. W.; Horrocks, W. D., Jr.; Young, V. G., Jr.; Rheingold, A. L.; Francesconi, L. C.; Antonio, M. R. *Inorg. Chem.* **2001**, *40*, 1894. (c) Zhang, C.; Howell, R. C.; Luo, Q.-H.; Fieselmann, H. L.; Todaro, L. J.; Francesconi, L. C. *Inorg. Chem.* **2005**, *44*, 3569. (d) Boglio, C.; Lenoble, G.; Duhayon, C.; Hasenknopf, B.; Thouvenot, R.; Zhang, C.; Howell, R. C.; Burton-Pye, B. P.; Francesconi, L. C.; Lacote, E.; Thorimbert, S.; Malacria, M.; Alfonso, C.; Tabet, J.-C. *Inorg. Chem.* **2006**, *45*, 1389.
(47) (a) Antonio, M. R.; Soderholm, L.; Williams, C. W.; Ullah, N.; Francesconi, L. C. *J. Chem. Soc., Dalton Trans.* **1999**, 3825. (b) Williams, C. W.; Antonio, M. R.; Soderholm, L. *J. Alloys Compd.* **2000**, *303*, 509. (c) Soderholm, L.; Antonio, M. R.; Skanthakumar, S.; Williams, C. W. *J. Am. Chem. Soc.* **2002**, *124*, 7290. (d) Lis, S.; But, S.; Klonkowski, A. M.; Grobelna, B. *Int. J. Photoenergy* **2003**, *5*, 233. (e) Lis, S.; But, S.; Meinrath, G. *J. Alloys Compd.* **2004**, *374*, 366.
(48) Evans, W. J. *Inorg. Chem.* **2007**, *46*, 3435.

In the reduced form, the average orbital energy of the 4f shell in the Ce-Preyssler complex is still very low (ca. −4.2 eV). This indicates that the oxidation state +3 could be stable enough inside the Preyssler cavity. The reduced state with the lowest energy is a non-aufbau state in the DFT calculation (see right column in Figure 7A). Forcing this electron in any other 4f orbital gives states with a higher energy. To make sure that this is not an artifact of the method, we performed CASSCF calculations with the MOLCAS program package.[49] The target atom, Ce, was computed at the quantum mechanical level, as well as the five PO_4 units surrounding it. The rest of the structure was included with point charges to reproduce the correct electrostatic field around the Ce. The active space contains seven orbitals and one electron. The orbitals were optimized for the seven states of the ^2F manifold. We used all electron basis sets for Ce (8s, 7p, 5d, 4f), O (3s, 2p), and P (4s, 3p).[50] Scalar relativistic effects are accounted for through the Douglas−Kroll Hamiltonian. These post Hartree−Fock calculations also located the unpaired electron in an almost pure Ce-4f(z^3) orbital for the lowest N-electron state. The atomic Ce^{III} ^2F state is split in seven nondegenerate states by the weak ligand field. The splitting is not larger than 1000 cm^{-1}. The inclusion of spin−orbit coupling[51] does not affect the character of the ground state but splits the seven ^2F states in two groups corresponding to the $^2F_{5/2}$ and $^2F_{7/2}$ terms. The splitting between these two groups is ∼2000 cm^{-1}, close to the experimental spin−orbit splitting in the Ce^{3+} ion.

The above statements might be reinforced by analyzing a differently behaving Ce−POM-like complex, such as $[Ce^{III/VI}(W_5O_{18})_2]^{9/8-}$ (Ce-Lindqvist).[45] This complex consists of two lacunary Lindqvist units linked by a Ce atom. Ce^{III} and Ce^{IV} oxidation states have been observed in this complex, which makes it different from Ce-Preyssler. DFT calculations result in a similar sequence of molecular orbitals as that for Ce-Preyssler, with the insertion of the empty 4f shell of Ce between the oxo and W bands (thick lines in Figure 7B).[52] However, the HOMO is somewhat higher in energy than that in Ce-Preyssler, and the Ce^{IV} 4f orbitals lie 1 eV above it, a sign of greater stability with respect to the situation of the Ce-Preyssler. To explain this, we explored the most relevant differences in the neighborhood of Ce. The Ce−O distance (2.52 Å) is 0.2 Å shorter than that in the Ce-Preyssler case, and the Ce is coordinated by eight oxygens. Both factors imply that the Ce-Lindqvist has stronger Ce−O bonding, which explains the higher energy of the Ce-4f empty orbitals (−4.66 eV) and their antibonding Ce−O character (90% Ce(4f), 10% O(p)). The energy range of Ce-4f orbitals suggests that both Ce^{III} and Ce^{IV}-Lindqvist are energetically possible, while the very low orbital energies in Ce^{IV}-Preyssler indicate that only the Ce^{III} form is energetically stable. The conclusion that longer Ce−O distances favor the Ce^{III} state was pointed out by Francesconi and coworkers.[47a] We also performed an exhaustive structure search in the Cambridge Structural Database for the Ce-containing POM and non-POM complexes.[53] Among these, d(Ce−O) values in the range 2.5−2.9 Å correspond to Ce^{III} cations, whereas distances of 2.2−2.4 Å were found in Ce^{IV} structures.

Not only Ce encapsulated in Preyssler clusters prefers lower oxidation states than those in other POM structures, but also the reduction of Eu^{3+} to Eu^{2+} occurs in the Eu-Preyssler system, while this process has not been reported in any other Eu−POM structure. Therefore, the lower oxidation state found for Ce in the Preyssler cluster seems to be related to its poor coordination. These facts may, via the energy of the molecular orbitals, also determine the oxidizing power of such complexes. For instance, the reduction energies computed in solution for the Ce-Lindqvist and Ce-Preyssler complexes are −3.46 and −5.40 eV, respectively. The latter reduction energy is even more negative than that of α-$S_2Mo_{18}O_{62}^{4-}$ (computed in our group to be −5.10 eV), one of the most oxidant POM known.[54] This evidences that the oxidation state of Ce is III. As a matter of fact, experimentalists[17a,47a] did not observe any Ce(III/IV) oxidation wave up to +1.9 V for this complex, indicating that oxidation of Ce^{III} would occur beyond that value. Regarding Pope's statements in his 1993 paper,[17a] Ce^{IV} could have been reduced along the preparation process of Ce-Preyssler.

Conclusions

DFT calculations were carried out on the so-called Preyssler anion, $[X^{n+}P_5W_{30}O_{110}]^{(15-n)-}$, which is the smallest polyoxometalate (POM) with an internal cavity allowing cation exchange with the solution. The cation release studied for the series of X^{n+} presents notable energy barriers, ranging from 30 kcal mol^{-1} for Na^+ to 50 kcal mol^{-1} for Th^{4+}. The energy cost for the cation encapsulation mainly depends on the dehydration energy of each X^{n+} since the necessary loss of the solvation sphere is a very endothermic process, explaining the high temperatures necessary for the encapsulation of the most charged cations.

The first one-electron reduction energies of the POM depend linearly on the internal X^{n+} charges. The computed slope is 48 meV per unit charge, in good agreement with the experimental 41 mV in the reduction potentials. Both protonation and cation encapsulation shifts the potential toward more positive values, but this effect is about *three times* larger for protonation. The most basic oxygen site is the internal oxygen bound to a P atom. Protonations at the external bridging W−O−W and O═M sites are +21 and +27 kcal mol^{-1} less favorable than the former. Indeed, the last proton's $pK_a = 2$ value for the Na^+ derivative was computed in good agreement with experiments.

Calculations performed for lanthanide−POM complexes reveal a higher complexity in the electronic structure, with the insertion of the empty 4f shell of the Ln cation between the oxo and W bands. In $CeP_5W_{30}O_{110}$, we observe that Ce is poorly coordinated to its nearest environment, influencing the Ce-4f orbital energies and thus making the oxidation state +3 the preferred one for cerium. The $Ce^{IV}PA^{11-}$ form resulted so highly oxidizing that it is energetically forbidden. In general, this would be the reason why most rare earths incorporated into Preyssler anions do not feature their highest oxidation states.

(49) Karlström, G.; Lindh, R.; Malmqvist, P. Å.; Roos, B. O.; Ryde, U.; Veryazov, V.; Widmark, P. O.; Cossi, M.; Schimmelpfennig, B.; Neogrady, P.; Seijo, L. *Comput. Mater. Sci.* **2003**, *28*, 222.
(50) Roos, B. O.; Lindh, R.; Malmqvist, P.-Å.; Veryazov, V.; Widmark, P.-O. *J. Phys. Chem. A* **2005**, *108*, 2851.
(51) Malmqvist, P.-Å.; Roos, B. O.; Schimmelpfennig, B. *Chem. Phys. Lett.* **2002**, *357*, 230.
(52) In both the Ce^{III}- and Ce^{IV}-Lindqvist complexes, the first unoccupied W-like molecular orbital is delocalized over the two equivalent W_4 rings.
(53) Allen, F. H. *Acta Crystallogr.* **2002**, *B58*, 380.
(54) (a) Zhang, J.; Bond, A. M.; MacFarlane, D. R.; Forsyth, S. A.; Pringle, J. M.; Mariotti, A. W. A.; Glowinski, A. F.; Wedd, A. G. *Inorg. Chem.* **2005**, *44*, 5123. (b) Mariotti, A. W.; Xie, J.; Abrahams, B. F.; Bond, A. M.; Wedd, A. G. *Inorg. Chem.* **2007**, *46*, 2530.

Acknowledgment. This work was supported by the Spanish MEC (CTQU2005-06909-C02-01/BQU and CTQU2005-08459-C02-02/BQU) and the DGR of the Autonomous Government of Catalonia (2005SGR-00104). J.A.F. is indebted to the Spanish MEC for a grant. Dedicated to Michael T. Pope in occasion of his retirement. The authors thank the reviewers' helpful comments on the manuscript.

Supporting Information Available: *XYZ* coordinates for several optimized structures, calculated absolute HOMO and LUMO energies and H−L gaps for $[XP_5W_{30}O_{110}]^{(15-n)-}$ and $[|XH_2O|P_5W_{30}O_{110}]^{(15-n)-}$, 3D representation of the LUMO, LUMO + 1, and LUMO + 2 of $[NaPA]^{14-}$, molecular orbitals scheme for the $[X^{n+}PA]^{q-}$ anions and $[|NaH_2O|PA]^{14-}$ and decomposition of the total interaction energy (in eV) for the $NaPA^{14-}$ and $ThPA^{11-}$ Preyssler-type polyoxoanions. This material is available free of charge via the Internet at http://pubs.acs.org.

JA0737321